Journal of Materials Chemistry A

Accepted Manuscript

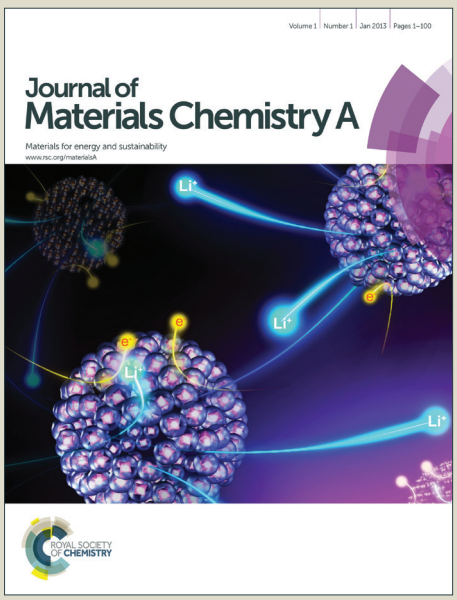

ROYAL SOCIETY OF CHEMISTRY

www.rsc.org/materialsA

Pristine and Defect Phophorene as Promising Anode Materials for Rechargeable Li Batteries

Gen-Cai Guo[1,2], Xiao-Lin Wei[1*], Da Wang[2], Yanping Luo[1], Li-Min Liu[2*]
[1]*Hunan Key Laboratory for Micro-Nano Energy Materials and Device, Department of Physics, Xiangtan University, Hunan, 411105, China*
[2]*Beijing Computational Science Research Center, 3 Heqing Street, Haidian District, Beijing 100084, China*
Email: limin.liu@csrc.ac.cn; xlw@xtu.edu.cn

Abstract

The pristine and defect phosphorene as a promising anode material for Li-ion batteries (LIBs) are systematically investigated by the first-principles calculations. The results suggest that the binding energies of Li adsorption on the different sites vary within a narrow range, and the binding between Li atom and pristine phosphorene is relatively weak. Interestingly, the defect can greatly improve the performance of the phosphorence in both binding energy and diffusion of Li on phosphoren. The binding energy of Li around the vacancy is increased by about 1 eV compared to that of the perfect phosphorene. More importantly, Li atoms could diffuse between two adjacent grooves with an energy barrier of 0.13 eV, which opens a novel channel for Li diffusion. This would dramatically improve the fast charge/discharge capability. These outstanding properties indicate that the defect PP has the great potential to be a good electrodes material in LIBs.

Keywords: black phosphorus, phosphorene, defect, binding energy, diffusion path, Li-ion batteries

1. INTRODUCTION

The rapid development of the electronic market reveals a breakthrough in terms of electrode materials in recent years. Lithium-ion rechargeable batteries, owning high reversible capacity[1, 2], high energy density[3, 4] and good cycle life[5], are used as portable power sources for plenty of electronic devices, such as cellular phones, notebook computers, and camcorders.[6, 7] Graphene are commonly used as a negative electrode for Li-ion batteries due to their large surface-to-volume ratio and special electronic properties differ from their bulk counterparts.[8-10] However, poor capacity (372 mA h g^{-1}) and weak binding with Li of graphene limit its application in Li-ion batteries (LIBs).[11-13] Other graphene-like two-dimensional materials, such as layered transition metal dichalcogenides and MXenes (M=Ti, V, Cr, Nb, etc. X=C, N) are also widely studied.[14-18] In view of their flat structures, fast Li diffusion and a large Li capacity can be achieved. [19, 20] It is still a challenge to obtain a satisfactory electrode with the good electrical conductivity, excellent cycling stability and rate capability.

Black phosphorus (BP) was first produced by Bridgeman in 1914,[21] it has recently attracted huge attention due to its graphite-like multi-layered phosphorene structure. BP consists of phosphorus atoms stacked in puckered layers, in which each phosphorus atoms is covalently bonded with three adjacent phosphorus atoms to form a puckered honeycomb structure.[22, 23] This structure makes BP more stable than white phosphorus and red phosphorus under normal conditions. Recently, the phosphorus-graphene hybrid nanosheets have exhibited exceptional high-temperature cycling stabilities as lithium-ion anode.[24] Similar to the graphite, the layered structure of black phosphorus also composes of a six membered phosphorus ring with an interplanar distance of 3.09 Å.[25, 26] In addition, because of the flat structures of BP, a fast Li diffusion and large Li capacity can be achieved for lithium intercalation. The theoretical specific capacity is 2596 mA h g^{-1} in the case of the uptake of lithium to the final composition of Li_3P.[27, 28] These outstanding feature leads BP to a promising negative electrode material for LIBs. However, for bulk BP, the cycling efficiency is limited due to large volume change in the lithiation process. Sun et al. reported that the volume change is around 300% upon lithiation.[29] This large volume expansion always results in rapid capacity fading.

Until now, the single-layered BP called phosphorene has been successfully fabricated, which has an atom-thick layer of the element phosphorus with a natural band gap.[18, 19, 30] Similar to graphene, phosphorene atoms are arranged hexagonally, while its surface is slightly puckered. It is still flat enough to confine electrons so that charge flows quickly, giving rise to a promising material by electrical engineers. Furthermore, the puckered honeycomb structure of phosphorene leads it to accommodate more Li atoms compared with bulk BP. Beyond that, since phosphorene is rather robust, the structural degradation is insignificant during the lithiation process, indicating the good cycle performance. Zhao *et al.*[31] Employed first-principles calculations to investigate the adsorption and diffusion of Li on phosphorene, they demonstrate that the theoretical specific capacity of the phosphorene monolayer can reach to 432.79 mA h g^{-1}, which is larger than those commercial anode materials, such as 372 mA h g^{-1} of graphite. However, the binding between Li atom and phosphorene

is weak. Meanwhile, the defect effect on phosphorene has not been taken into account in the previous studies, though it is inevitable in experimental preparation. Thus, it is greatly necessary to uncover the defect effect on the electrochemical properties of phosphorene.[32, 33]

In our work, we investigate the adsorption and diffusion properties of Li atom on both pristine phosphorene (PP) and single vacancy defect phosphorene (SVP) systematically. The results suggest that defect can greatly improve the performance the electrochemical properties of phosphorene. The Li atoms bond stronger at the defect sites than that in perfect phosphorene. Moreover, the diffusion barrier of Li atom between two adjacent grooves greatly decreases to 0.13 eV, indicating the inter-diffusion of Li atoms between two adjacent grooves becomes possible. Our results provide a theoretical guidance for the experimental preparation of high-performance phosphorene as LIBs.

2. COMPUTATIONAL METHODS

All the calculations were carried out using DFT calculations as implemented in the Vienna ab initio package (VASP) with a plane wave basis set.[34, 35] The projector augmented wave (PAW) method was applied to describe the electron-ion interactions, while the exchange correlation energy was described by the scheme of Perdew-Burke-Ernzerhof (PBE) in generalized gradient approximation (GGA).[36] In addition, the electron wave functions were expanded by a plane wave cutoff of 360 eV. The calculation was performed on *a 4a ×1b×4c* (a, b and c are the lattice constants of black phosphorus) cell for PP and SVP, and a 20 Å vacuum layer is used to simulate the adsorption and diffusion of Li on the PP and SVP. G-point sampling for the Brillouin zone integration is used. Meanwhile, the energy convergence with the energy difference is below 10^{-5} eV between two consecutive self-consistent steps while the positions of all the atoms in the supercell were fully relaxed until the force was less than 10^{-2} eV/A.

To study the Li diffusion kinetics, activation barriers were calculated using the climbing image nudged elastic band (CI-NEB) method.[37] The CI-NEB is an efficient method to determine the minimum energy path and saddle points between a given initial and final positions. Structures of initial and final points were first fully optimized before the CI-NEB calculation. After that, six or twelve intermediate images were linearly interpolated between them. Each image searched for its potential lowest energy configuration along the reaction path while maintaining equal distance to nearby images. CI-NEB calculation of the SVP was performed based on similar details and conditions described above.

The binding energy is defined by the following equation[11]

$$E_b = (E_{PP/SVP} + nE_{Li} - E_{PP/SBP+Li_n})/n$$

Where $E_{PP/SVBP}$ is the total energy of the pristine phosphorene/single vacancy phophorene, $E_{PP/SVP+Li_n}$ is the total energy of phosphorene/single vacancy

phophorene with adsorbed n Li atoms and E_{Li} is the energy of an isolated Li atom. A positive E_b represents that Li atoms tend to bind to the phosphorene/single vacancy phophorene, which indicates a more favorable exothermic lithiation reaction. Under this definition, a higher value of E_b means stronger binding between Li and phosphorene/single vacancy phophorene.

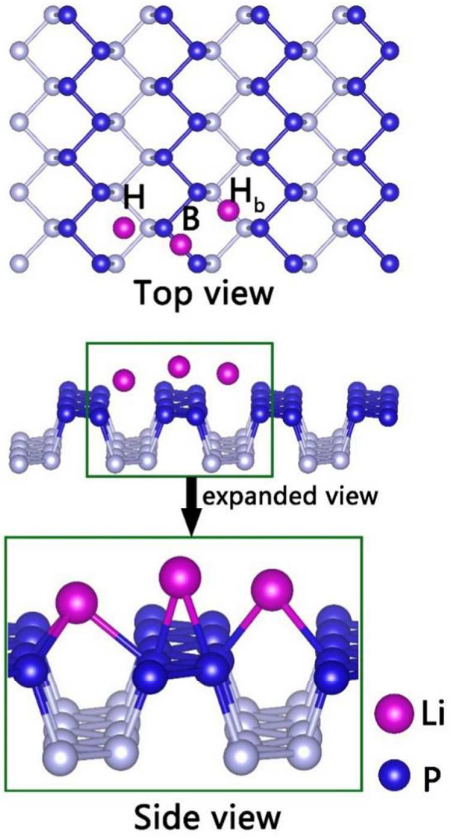

Figure 1. *Top and side view of three possible adsorption sites (1) H site; (2) H_b site; (3) B site.*

3. RESULTS AND DISCUSSION

3.1 Li adsorption and diffusion on the pristine phosphorene

3.1.1 Li Adsorption on PP

We first consider the electrochemical properties of pristine phosphorene (PP). The calculated bond length and band gap value of PP are 2.22 Å, 2.22 Å, 2.25 Å, and 0.95 eV, respectively, which are consistent with previous studies.[22, 38] In order to examine the energetic stability of Li atoms on PP, several possible Li adsorption sites on the PP were considered: (1) H sites: above the center of the triangle consisting of three P atoms in the surface; (2) H_b sites: above the mid-point of P-P bond in the bottom phosphorus atoms; (3) B sites: above the mid-point of P-P bond in the top phosphorus atoms, as shown in **Figure 1**.

We performed a full geometry optimization for the structure of Li adsorption on PP, as shown in Figure 1. The calculated results show that the H configuration is more

stable than other cases and the bond length of absorbed Li with three nearest P is 2.55 2.55 and 2.45 Å, respectively, which are consistent with previous theoretical calculations.[31, 39] To understand the electrochemical properties of different lithiated phase during the lithium extraction/intercalation process, the stable crystal structure of Li_xP_{64} (X=8, 16 and 32) in the process of lithium intercalation was firstly explored. For each concentration, we calculated several different potential configurations. The geometries with the maximum binding energy are listed in **Figure 2**, and some characteristics are found. Firstly, neither of the Li atoms would stay at the same six membered phosphorus ring due to the electrostatic repulsion between Li atoms and material distortion. Furthermore, the configurations with the equal number of Li adatoms at the upper and lower surface have the lowest formation energy than the unequal case. Finally, the corresponding binding energy gradually decreases with the increase of Li adatoms, indicating a descending of thermodynamic stability during the lithiated process.[40] The reduction in binding energy can be attributed to the two main factors. The first is the weak electrostatic attraction between phosphorene host and Li cations. The other is the enhanced Li-Li repulsion at the relatively high Li concentrations.

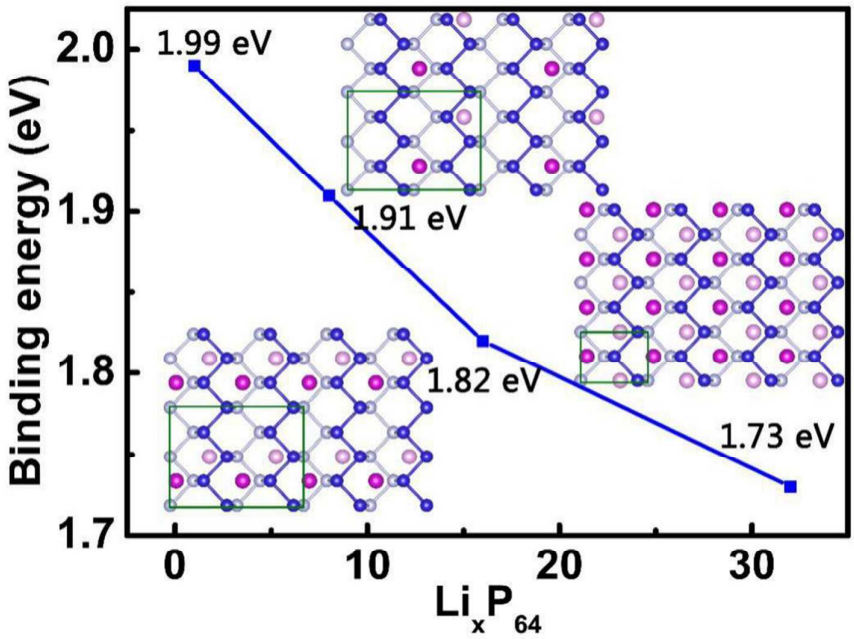

Figure 2. *The binding energy of x Li atoms adsorbed on PP (x=1, 8, 16, 32). The optimized stable configuration of Li_xP_{64} (x=8, 16, 32) is shown as well.*

As the additional Li atoms embedded into the $Li_{32}P_{64}$ system, the additional Li atoms will be pushed out of the surface due to the repulsion between the Li atoms in the first nearest Li layer. In this case, the distance from additional Li adatoms to PP's surface is 2.38 Å, which is larger than the average distance of 32 Li (viz. 1.596 Å), and the configuration become disorder, meaning the bonds between Li atom and PP break. As discussed above, the maximum Li adsorbed atoms were predicted to be $Li_{32}P_{64}$, corresponding to a Li storage capacity of 432.79 mA h g^{-1}. Here, it is worth

noting that with the increasing number of Li atoms, the geometry changes of all $LixP_{64}$ configurations are negligible (less than 1.3%) while the binding energy of all Li concentrations are also varied in a narrow range, as shown in **Figure 2**, which suggests a commendable stability. As the number of adsorbed Li atoms reached to 64 with every H site filled, a phase transformation occurs. In the transformed phase (LiP), P atoms connected in chains along the b-axis, and cleaved along the a-axis by Li atoms during discharge (**Figure S1**), which is also reported in the previous experimental study. [41, 42] Although the Li atom adsorption is considered in our calculation, once upon the Li atom adsorption on P substrate, the Li atom becomes Li cation.

3.1.2 Electronic Properties

In order to get a further understanding of the interaction between Li and PP, we investigate the density of state of $LixP_{64}$ (X =1, 16 and 32), as shown in **Figure 3**. For pristine phosphorene, the states near the Fermi levels are mainly dominated by P (3*p*) states.[31] After Li adsorption on PP, the Li/PP system becomes metallic, indicating electron transfer from Li atoms to PP. This phenomenon is also found in graphene, which turns from semi-metal to metallic after lithiation.[43] Recently, a research group show that small molucules adsorption can affect the electronic properties of phosphorene.[44] In addition, it can be seen (see **Figure 3**) that the conduction band proportions of Li states reduce with the increase of Li adatoms, which implies that the charge transfer decreased slightly and the stability of the system is weakening. It should be noted that the transition from semi-conduction to metallic has significant effect for its application in LIBs. Besides, the PDOS that the Li orbitals overlap with PP, indicting their covalent hybridization interactions. Although the bond between Li and PP is dominated by the ionic interactions, some covalent components still cannot be ignored.

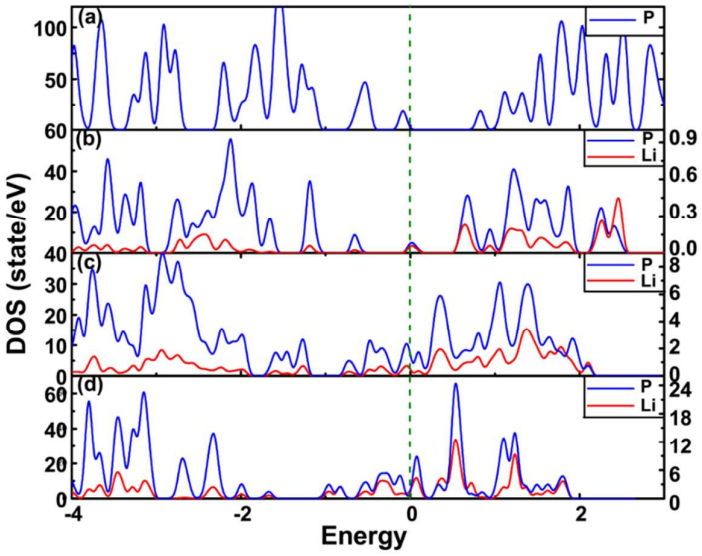

Figure 3. *(a), (b), (c) and (d) represent the density of state of 0, 1, 16, and 32 Li atom adsorptions on PP, respectively. The blue line represent the PDOS of pure PP, the red line represent the PDOS of Li.*

In an effort to quantitatively estimate the amount of charge transfer between the adsorbed Li and PP, Bader charge analysis were calculated for all the compositions.[45, 46] As one Li atom adsorbed at the H site, the corresponding charge of Li is +0.865|e|, while the charge of three nearest neighbor P atoms next to Li is calculated to be -0.230|e|, -0.214|e| and -0.258|e|, respectively. The results reveal that the interaction between the adsorbed Li atom and P atoms is predominantly ionic, where the valence electrons from the adsorbed Li atoms transferred to the nearest neighbor P atoms. In addition, the charges of Li with the number of 8, 16 and 32 is +0.855|e|, +0.848|e| and +0.793|e|, respectively. These changes reveal that less electrons of Li atoms transfer to P substrate, indicating the weaker ion bonds formed with the increase of Li-adsorption. Furthermore, the large electron transfer indicates that the Li atoms are strongly polarized after adsorption and the Coulomb force dominates the interactions between Li and phosphorene. We have calculated the spin electronic state, and show that the entire configurations are nonmagnetic. We also calculate the maximum voltage and the average voltage of Li adsorption on pristine phosphorene, which is 0.38 V and 0.12 V based on the adsorption energies, respectively. This result shows a moderate open circuit voltage of phosphorene to use as the anode material for Li-ion battery anodes.

3.1.3 Li Diffusion Process

The intrinsic Li mobility on the PP is vital for the actual application as an anode material of LIBs. Thus we studied the possible diffusion path and energy barrier of Li on PP, as shown in **Figure 4**. The most stable adsorption site for Li is H sites. As Li moves between two adjacent H sites, two potential paths exist (anisotropic diffusion

barrier): H-H_b-H (inside the groove), and H-B-H (between two adjacent grooves), where H_b and B are transition states. The diffusion barriers along H-H_b-H and H-B-H direction are 0.09 eV and 0.65 eV, respectively, which is consistent with previous study and suggesting that Li can diffuse faster along the groove than between two adjacent grooves, like the water flow inside the groove.[39]

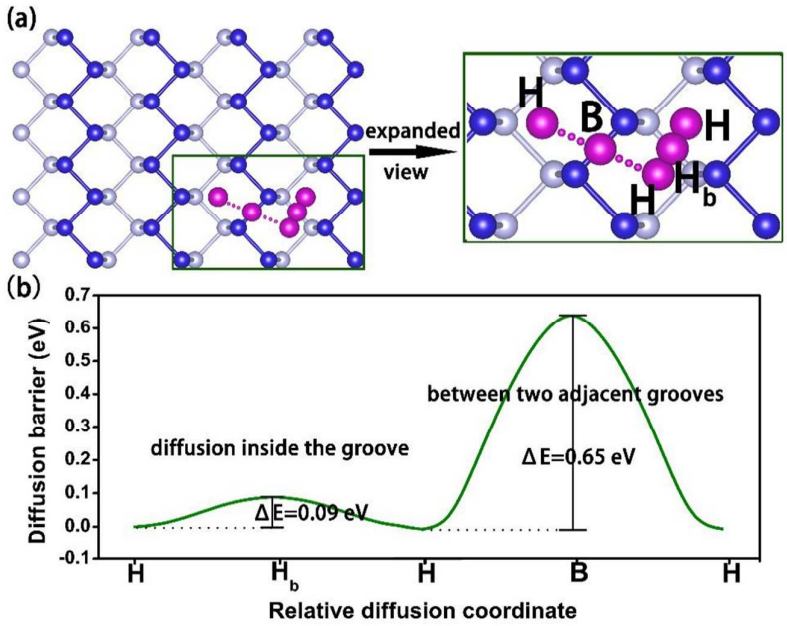

Figure 4. *Energy barrier and diffusion path of one Li atom move on the PP. (a) Diffusion path between two H sites; (b) Diffusion barrier between two H sites. The H_b and B are represent the intermediate state.*

3.2 Li adsorption and diffusion on the defect PP

As discussed above, the pristine phosphorene with high Li mobility have great potential to be used as the anode materials for LIBs. However, the weaken Li bonding strength of phosphorene essentially limit their electrochemical performances. We next turn to study the structural and electronic characteristics of single vacancy defect phosphorene (SVP), as well as their improvement on the electrochemical properties.

3.2.1The SVP structure

We first performed a fully geometry optimization for single vacancy structure after removing one P atom from PP. Due to the equivalency of all the P atoms, there is only one kind of single vacancy configuration before reconstruction. Our calculations show that there are two possible stable single vacancy configurations after reconstruction. To begin with, a bottom P atom moves upward slightly, the moved bottom P atom bonding with two top adjacent P atoms and two bottom adjacent P atoms forming four pentagons, as shown in **Figure 5a**. Besides, a configuration with octatomic ring is obtained which has a dangling bond in the upper P atom, as illustrated in **Figure 5b**, and it is more stable than the configuration that with four

pentagon. The DOS of SVP is also given in **Figure 5c** and **5d**. It can be seen that the four pentagon configuration has a p-type state and without magnetic (**Figure 5c**) while in the octatomic configuration, the Fermi level is located in the valence band and the vacancy create a spin-polarized p-type state (**Figure 5d**) due to the presence of dangling bonds. This might be the origin of p-type conductivity observed experimentally in 2D P.[22, 23, 47] Thus, we adopt the structure that with octatomic ring in the following calculation.

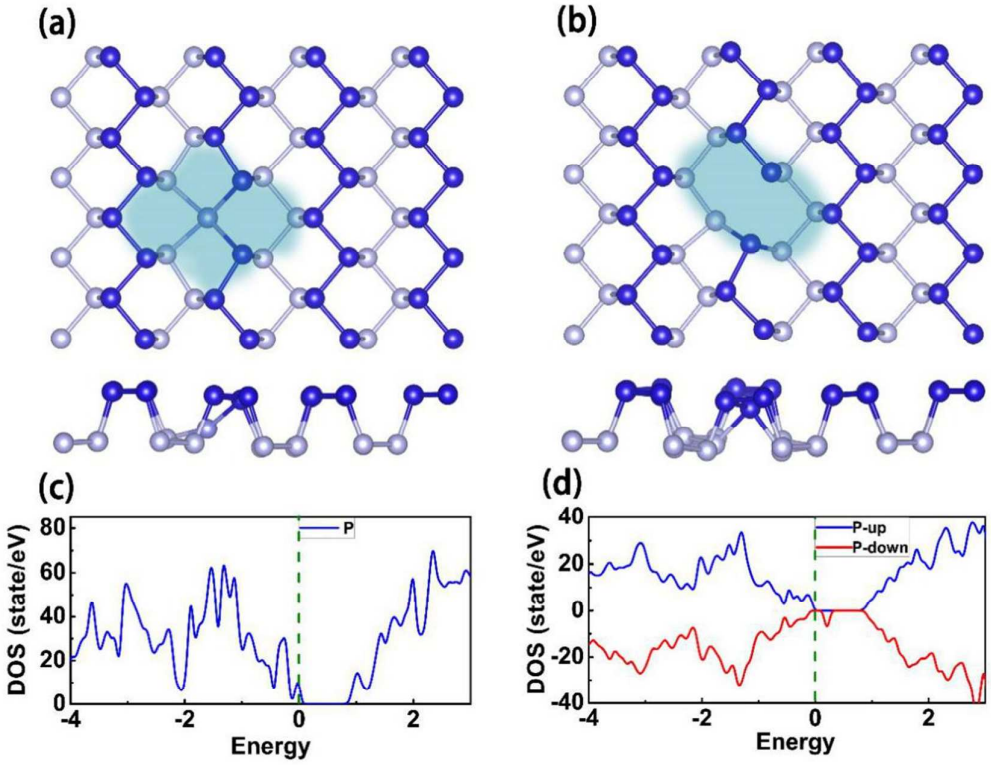

Figure 5. *Stable configuration and DOS of SVP. (a), (c) The configuration of four pentagon and corresponding DOS, respectively. (b), (d) The configuration of octatomic ring and corresponding DOS, respectively.*

3.2.2 Li Adsorption on SVP

In order to examine the influence of one single vacancy defect in phosphorene, different Li adsorption positions around the single vacancy were considered. The stable structure after Li atom adsorbing in SVP around the defect are shown in **Figure 6**, and the corresponding binding energy is listed in **Table 1**. The binding energies vary slightly (within 0.1 eV) with the different adsorption sites. Compared with the PP, the most stable adsorption site of SVP is still the H site out of the vacancy. We note that Li atoms are inclined to occupy the sites around vacancy at first, and then hold the pristine H sites in the next stage. The binding energies of Li in SVP were calculated to be ranged from 3.00-3.31 eV, which were greatly enhanced compared with PP (1.99 eV). Moreover, the changes of volume is trivial (less than 2%) after Li atom inserts into the SVP, suggesting the excellent ability to resist volume change as

an anode material.

3.2.3 Electronic Properties

To uncover the different binding strength of Li on the defect sites of SVP, we calculated the charge density difference from the following equation for Li atom located on the SVP,[48]

$$\Delta\rho(\mathrm{r}) = \rho_{Li-SVP}(r) - \rho_{SVP}(r) - \rho_{Li}(r),$$

Where $\rho_{Li-SVP}(r)$ represents the charge density of Li adsorbed SVP system, $\rho_{SVP}(r)$ is the charge density of the SVP and $\rho_{Li}(r)$ is the charge density of isolated Li atoms in the same position as in the total systems. Figure 6a show the charge density difference of Li atoms adsorbed on H_1 and H_3 site of SVP, and the cases of Li adsorbed on other sites are also shown in **Figure S2**. Loss of electrons is indicated in blue and gain of electron is indicated in yellow. It can be seen from **Figure 6a** that a net loss of electronic charge were found just above the Li and also a net gain of electronic charge were found on their adjacent P atoms, indicating the electrons transfer from Li atom to adjacent P atoms to form a strong ionic bond, and the Li atoms are strongly polarized after adsorption. In addition, it is noted that the closer of Li atoms to the vacancy, the more electrons transfer from Li to P atoms. This is mainly due to the saturation of dangling bond by adsorbed Li atom, which makes Li atom bonding more strongly with the SVP. As for H_1 site (**Figure 6b**), the adsorbed Li atom is out of the vacancy, and the dangling bond still exists In this case, the electronic from Li atom transfer to four neighbor P atoms to form ionic bonds. However, in H_3 Li-adsorption configuration (**Figure 6b**), the adsorbed Li atom is around the vacancy so that the dangling bond bonds with the Li atom. The large charge gains demonstrate the significant electronic transfer from Li atom to three neighbor P atoms, indicating the strong bonding of the adsorbed Li atom with three neighbor P atoms. The large electron transfer indicates that the Li atoms are strongly polarized after adsorption. Similar with PP, we have also carried out spin-polarized calculation to explore possible magnetic ground states and our result reveals that all the adsorption configuration are nonmagnetic. As shown in **Table 1**, the closer of Li adatoms to the vacancy, the stronger bonding they are. Moreover, It should be noted that the covalent components between Li and the SVP still cannot be ignored, which is similar with the PP case as mentioned before.

Since the pristine SVP is a p-type doped semiconductor, as one Li atom adsorbed on the SVP, dangling bond was filled at first. The continually increase of adsorbed Li atoms would lead to the semiconducting to metallic transformation. This transformation would have significant effects for its application in LIBs.

Table 1 Binding energy and Bond length for Li atom adsorption on the different sites of SVP

Adsorption site	H_1	H_2	H_3	H_4	H_5	H_6	I_1
E_b (eV)	3.00	3.28	3.31	3.18	3.31	3.18	3.14
Bond length (Å)	2.55	2.49	2.48	2.52	2.48	2.52	2.53

3.2.4 Li Diffusion Process

Since the capacity of rapid charge and discharge is closely linked with the diffusion properties, we next turn our attention to the mobility of Li atoms in SVP structure. We first studied the possible diffusion path and energy barrier of Li atom on SVP, there is two possible diffusion paths: (I) Li atom diffusion inside the groove, and (II) Li atom diffusion from one groove to the adjacent one.

For the case of Li atom diffusion inside the groove, the diffusion path is along the direction 1 (H_1-H_2-I_1) (**Figure 6c**). The results show that Li atom firstly diffuses from H_1 site to H_2 site with an energy barrier of 0.10 eV. As Li atom further diffuses through the vacancy, it will adsorb on I_1 site to form a new configuration with an energy barrier of 0.17 eV, which is a little larger than the one of Li atom diffusion between two H sites in PP (0.09 eV). When Li atom diffuses between two adjacent grooves, two possible diffusion paths were found, as shown in **Figure 6**. One is along the direction 2 (H_1-H_2-H_3-H_4) (**Figure 6a**), and the other is along the direction 3 (H_1-H_2-H_3-H_5-H_6) (**Figure 6d**).

We note that when Li reached to H_2 site, it may cross the groove (direction 3) reach to another stable site (H_3 site), which locates in the adjacent groove. In this case, the diffusion energy barrier is only 0.13 eV, which is greatly decreased compared with that in PP (0.65 eV). Interestingly, Li atoms may diffusion between the grooves by passing through the defects in SVP, while such diffusion cannot occur in PP due to the significant diffusion barriers. In the next stage, there have two possible diffusion ways of Li to diffuse away from the vacancy (direction 2 and 3). As Li diffusion from H_3 to H_4 site, a slightly larger barrier is found (0.22 eV), while it diffuses to H_5 more conveniently with an energy barrier of 0.07 eV. Then it diffuses to H_6 site, which is out of the vacancy, as shown in **Figure 6d**. In addition, we also explored the diffusion between two sides of the SVP, and a high energy barrier is found (1.07 eV). Overall, the above results imply that the introduction of single vacancy defect in phosphorene will open a channel for Li diffusion between two adjacent grooves, which make the Li diffusion more easily. Thus, we suggest that the high Li bonding strength and the convenience of Li diffusion through grooves indicate the higher stability and faster charge/discharge capability of SVP compared to phosphorene.

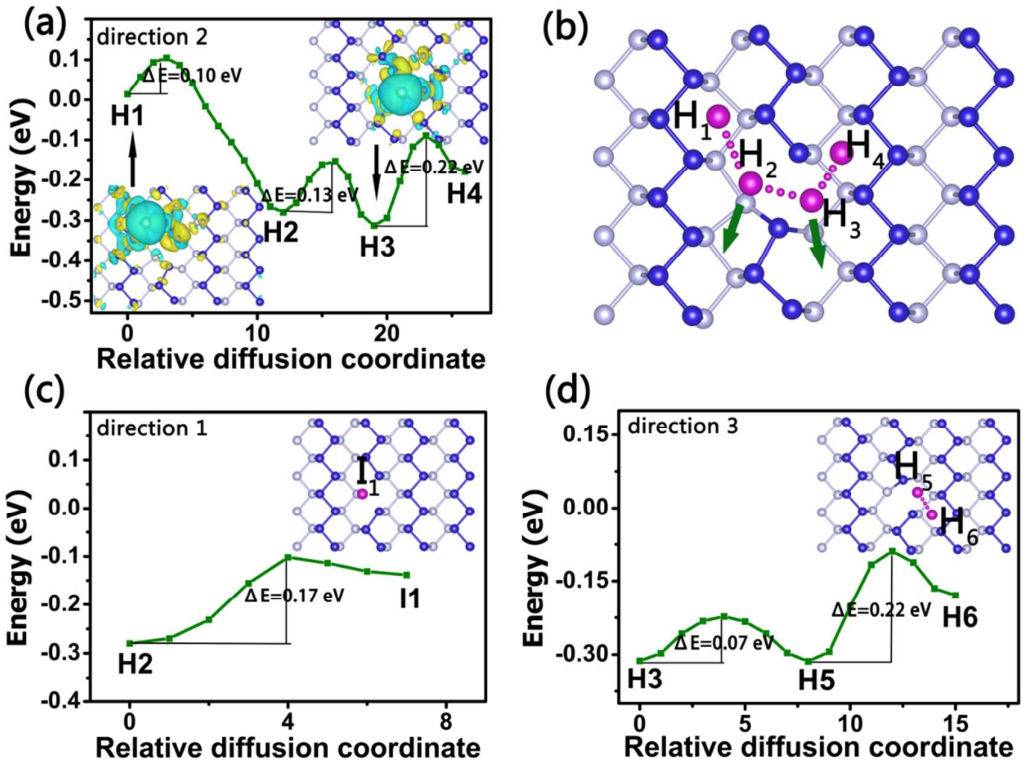

Figure 6. *(a) The diffusion barrier of Li atom on SVP (direction 2) and the charge density difference for Li adsorption on H_1 and H_3 sites. Yellow surfaces correspond to charge gains and blue surfaces correspond to an equivalent charge lost. (b) The adsorption site (H_1, H_2, H_3, and H_4) and diffusion path of Li atom on SVP. (c) The adsorption site (I_1) and diffusion barrier (direction 1). (d) The adsorption site (H_5, H_6) and diffusion barrier (direction 3).*

4. CONCLUSION

In this work, we systematically investigate the potential of pristine and defect phosphorenes as anode materials for Li-ion batteries based on first-principles calculations. Our calculated results reveal that the binding energy of Li on pristine phosphorene is relative weak (1.73 eV-1.99 eV), and the Li can only diffuse within the same channel, which greatly limits the performance of phosphorene as anode materials. Interestingly, defect phosphorene can not only improve the binding energy, but also diffusion ability. When the phosphorene contains vacancy, the Li atoms tend to occupy the site around the vacancy with the maximum binding energy of 3.31 eV, which is about 1 eV larger than in PP. More importantly, the results further reveal that the Li atoms could diffuse between two adjacent grooves in SVP with an energy barrier of 0.13 eV, which would dramatically improve the fast charge/discharge capability. These studies suggest that defect phosphorene can be used as an excellent electrode material in Li-ions batteries, which provide guidance on the preparation of high performance PP as LIBs in experiment.

Acknowledgments

This work was supported by the National Natural Science Foundation of China (No. 51222212, 11204262 and 51472209), the MOST of China (973 Project, Grant NO. 2011CB922200).the Program for Changjiang Scholars and Innovative Research Team in University (IRT13093).

REFERENCE

1. Y. Idota, T. Kubota, A. Matsufuji, Y. Maekawa and T. Miyasaka, *Science*, 1997, 276, 1395-1397.
2. E. Yoo, J. Kim, E. Hosono, H.-s. Zhou, T. Kudo and I. Honma, *Nano letters*, 2008, 8, 2277-2282.
3. J.-M. Tarascon and M. Armand, *Nature*, 2001, 414, 359-367.
4. N. Oyama, T. Tatsuma, T. Sato and T. Sotomura, 1995.
5. L. Ji, Z. Lin, M. Alcoutlabi and X. Zhang, *Energy & Environmental Science*, 2011, 4, 2682-2699.
6. Y. Wang and G. Cao, *Advanced Materials*, 2008, 20, 2251-2269.
7. G. Derrien, J. Hassoun, S. Panero and B. Scrosati, *Advanced Materials*, 2007, 19, 2336-2340.
8. K. S. Novoselov, A. K. Geim, S. V. Morozov, D. Jiang, Y. Zhang, S. V. Dubonos, I. V. Grigorieva and A. A. Firsov, *Science*, 2004, 306, 666-669.
9. A. K. Geim and K. S. Novoselov, *Nat Mater*, 2007, 6, 183-191.
10. Y. Jing, Z. Zhou, C. R. Cabrera and Z. Chen, *Journal of Materials Chemistry A*, 2014, 2, 12104-12122.
11. X. Fan, W. Zheng and J.-L. Kuo, *ACS applied materials & interfaces*, 2012, 4, 2432-2438.
12. X. Fan, W. Zheng, J.-L. Kuo and D. J. Singh, *ACS applied materials & interfaces*, 2013, 5, 7793-7797.
13. E. Pollak, B. Geng, K.-J. Jeon, I. T. Lucas, T. J. Richardson, F. Wang and R. Kostecki, *Nano letters*, 2010, 10, 3386-3388.
14. Y. Jing, Z. Zhou, C. R. Cabrera and Z. Chen, *The Journal of Physical Chemistry C*, 2013, 117, 25409-25413.
15. Y. Li, D. Wu, Z. Zhou, C. R. Cabrera and Z. Chen, *The Journal of Physical Chemistry Letters*, 2012, 3, 2221-2227.
16. H. Chen, J. Huang, X. Lei, M. Wu, G. Liu, C. Ouyang and B. Xu, *Int. J. Electrochem. Sci*, 2013, 8, 2196-2203.
17. Q. Tang, Z. Zhou and P. Shen, *Journal of the American Chemical Society*, 2012, 134, 16909-16916.
18. Y. Xie, M. Naguib, V. N. Mochalin, M. W. Barsoum, Y. Gogotsi, X. Yu, K.-W. Nam, X.-Q. Yang, A. I. Kolesnikov and P. R. Kent, *Journal of the American Chemical Society*, 2014, 136, 6385-6394.
19. C. Sun and D. J. Searles, *The Journal of Physical Chemistry C*, 2012, 116, 26222-26226.
20. H. Zhang, Y. Xia, H. Bu, X. Wang, M. Zhang, Y. Luo and M. Zhao, *Journal of Applied Physics*, 2013, 113, 044309.
21. P. Bridgman, *Journal of the American Chemical Society*, 1914, 36, 1344-1363.
22. H. Liu, A. T. Neal, Z. Zhu, Z. Luo, X. Xu, D. Tománek and P. D. Ye, *ACS nano*, 2014, 8, 4033-4041.
23. L. Li, Y. Yu, G. J. Ye, Q. Ge, X. Ou, H. Wu, D. Feng, X. H. Chen and Y. Zhang, *Nature nanotechnology*, 2014, 9, 372-377.

24. Z. Yu, J. Song, M. L. Gordin, R. Yi, D. Tang and D. Wang, *Advanced Science*, 2015, 2.
25. F. Xia, H. Wang and Y. Jia, *Nature communications*, 2014, 5.
26. R. W. Keyes, *Physical Review*, 1953, 92, 580.
27. M. C. Stan, J. von Zamory, S. Passerini, T. Nilges and M. Winter, *Journal of Materials Chemistry A*, 2013, 1, 5293-5300.
28. W.-J. Li, S.-L. Chou, J.-Z. Wang, H.-K. Liu and S.-X. Dou, *Nano letters*, 2013, 13, 5480-5484.
29. J. Sun, G. Zheng, H.-W. Lee, N. Liu, H. Wang, H. Yao, W. Yang and Y. Cui, *Nano letters*, 2014, 14, 4573-4580.
30. E. S. Reich, *Nature*, 2014, 506, 19-19.
31. S. Zhao, W. Kang and J. Xue, *Journal of Materials Chemistry A*, 2014, 2, 19046-19052.
32. J. Gao, J. Zhang, H. Liu, Q. Zhang and J. Zhao, *Nanoscale*, 2013, 5, 9785-9792.
33. X.-H. Zha, R.-Q. Zhang and Z. Lin, *The Journal of chemical physics*, 2014, 141, 064705.
34. G. Kresse and J. Furthmüller, *Physical Review B*, 1996, 54, 11169.
35. G. Kresse and J. Furthmüller, *Computational Materials Science*, 1996, 6, 15-50.
36. J. P. Perdew, J. Chevary, S. Vosko, K. A. Jackson, M. R. Pederson, D. Singh and C. Fiolhais, *Physical Review B*, 1992, 46, 6671.
37. G. Henkelman, B. P. Uberuaga and H. Jónsson, *The Journal of chemical physics*, 2000, 113, 9901-9904.
38. V. Tran, R. Soklaski, Y. Liang and L. Yang, *Physical Review B*, 2014, 89, 235319.
39. Q. Yao, C. Huang, Y. Yuan, Y. Liu, S. Liu, K. Deng and E. Kan, *The Journal of Physical Chemistry C*, 2015.
40. T. H. Osborn and A. A. Farajian, *The Journal of Physical Chemistry C*, 2012, 116, 22916-22920.
41. L. Cartz, S. Srinivasa, R. Riedner, J. Jorgensen and T. Worlton, *The Journal of Chemical Physics*, 1979, 71, 1718-1721.
42. C. M. Park and H. J. Sohn, *Advanced Materials*, 2007, 19, 2465-2468.
43. C.-K. Yang, *Applied Physics Letters*, 2009, 94, 163115.
44. Y. Jing, Q. Tang, P. He, Z. Zhou and P. Shen, *Nanotechnology*, 2015, 26, 095201.
45. G. Henkelman, A. Arnaldsson and H. Jónsson, *Computational Materials Science*, 2006, 36, 354-360.
46. S. Yang, D. Li, T. Zhang, Z. Tao and J. Chen, *The Journal of Physical Chemistry C*, 2011, 116, 1307-1312.
47. Y. Liu, F. Xu, Z. Zhang, E. S. Penev and B. I. Yakobson, *Nano letters*, 2014, 14, 6782-6786.
48. K. Persson, V. A. Sethuraman, L. J. Hardwick, Y. Hinuma, Y. S. Meng, A. van der Ven, V. Srinivasan, R. Kostecki and G. Ceder, *The journal of physical chemistry letters*, 2010, 1, 1176-1180.